

On the Surface of Topological Insulators: From Finite-Size Anomalous Currents to Potential Qubits

Alexander Selem*

*Department of Physics, University of California, Berkeley, CA 94720, USA and
Berkeley Quantum Information and Computation Center,
University of California, Berkeley, CA 94720, USA*

(Dated: August 24, 2022)

Results are presented for anomalous currents on the surface of topological insulators with ferromagnetic time-reversal breaking mass terms on fully closed topologies. Half-integer quantized Hall currents are computed using Dirac energy eigenstates on a flat torus (genus one topology) and closed cap cylinder (genus zero topology) with various massive regions and electromagnetic sources applied. Unlike the massive Dirac theory on an infinite plane with anomaly dependence $|m|/m$, one finds a smooth dependence when the mass-region strength is not infinite. This dependence could be measurable for typical ferromagnetic materials and crystal sizes. Issues related to charge transport, gap-crossing bands, and flux threading are discussed and clarified for different mass geometries. Finally, in light of the results for various mass configurations, a construction is proposed using ferromagnetic mass terms that can serve as a potential charged qubit.

PACS numbers: 71.10.Pm, 73.20.At, 73.43.-f, 03.67.Lx

I. INTRODUCTION

The surface of 3-dimensional topological insulators has been predicted and observed to contain an odd number of massless Dirac fermion modes.^{1–8} The 2+1 dimensional massive quantum Dirac theory is known to exhibit an anomalous contribution to the Hall conductance ($\hbar, c, = 1, e = |e|$) $\sigma_{xy} = \frac{m}{|m|} \frac{e^2}{4\pi}$,^{9,10} representing a half charge pumped contribution per unit of threaded flux in a Laughlin type set-up.^{11,12} In practice, nature presents other constraints for observing this half-quantization: namely a flat two dimensional lattice theory such as graphene, must have an even number of Dirac modes.^{13–15} Having effectively two or more pairs of fermion flavors, the half-integer quantization cannot be directly observed since the single fermion results are effectively doubled and Laughlin-type arguments are manifested in chiral energy bands at edges. In contrast, the surface of a topological insulator can have a single Dirac cone, however, it necessarily involves closed topologies. Furthermore, effective mass term(s) can be given to the surface theory in certain regions or along the entire surface, by coupling the surface to a ferromagnetic time-reversal breaking material.¹⁶ As such, the original inspiration of this paper is to investigate expected anomalous currents on closed surfaces and how the discontinuous mass dependence arises in conjunction with masses only partially covering the surface. Also, how does flux threading induce fractional charge pumping for various constructions? These topics will be the subject of Sec. II to Sec. IV.

In Ref. 17 the possibility of fractional charge accumulation was examined when a flux is inserted through a solid finite topological insulator sample. They found that inserting a flux tube into a topological insulator induces gapless states in the bulk of the material (along the flux), and separately a numerical calculation confirmed a

charge being transported through the flux tube. It was concluded that the surface theory is not robust to tunneling through the sample. The appearance of low energy modes was emphasized as responsible for discharging the ends of the flux tube which would otherwise be expected to contain localized fractional charges. However, this requires some clarification, and it is one of the purposes of this paper to do so. Namely, it is not possible to explain a half-charge quantized transport on the basis of bands traversing the gap. In fact, the dependence on the sign of the mass in the two dimensional plane result implies the existence of the current in a fully gapped theory. Instead the mid-gap states discussed in Ref. 17 is reminiscent of one of the cases considered below: the massless Dirac theory on a genus one torus. These aspects will further be discussed in Sec. IV A.

I will consider two exemplary geometries based on a cylindrically shaped topological insulator potentially realizable as a wafer sliced from a crystal boule. The first geometry examined (Sec. III) is intended to be prototypical for having a hole bored through the axis of symmetry so that its boundary has the topology of a genus one surface or torus. Aiming for simplicity in this first case, the edges will be smoothed to form a torus (see Fig. 1) which is further idealized as the flat torus. In this case, depending on the spin-structure the spectrum may be gapped even in the massless theory, but inserting a flux through the hole shifts the azimuthal quantum number allowing for a zero energy state at π flux (reminiscent of the discussion in Ref. 17). However there is *no* Hall conductance in this (massless) case. As the surface is coated with a mass, then a Hall conductance is generated, though the spectrum remains fully gapped throughout the entire flux cycle. The Hall current is computed directly by solving for the wavefunctions with electric fields inserted on the surface for different values of mass. Therefore the existence of an anomalous current is understood, but not

in terms of gap-crossing bands. Furthermore, it is found that the strength of the current *smoothly* goes from zero to full quantization as the mass is made stronger.

The second geometry solved for in this paper is a closed cylinder which remains effectively described by a surface Dirac theory even when fluxes are inserted through the material (see Fig. 7(b)). This geometry will be considered in section IV B with various surface mass terms to explore anomalous charge accumulation when a flux is inserted. Here again, one finds that if the mass-region is not sufficiently strong, the Hall current dependence on the mass is not the sharp $\text{Sign}(m)$, but rather changes smoothly. The mass-region is the mass times a characteristic length scale over which the mass term is present. Note that the sharp mass dependence agrees with the infinite plane since in that case the characteristic length is infinity, so that any finite mass for the fermion will lead to the full quantization.

Finally gaining intuition from different mass geometries computed, a potential configuration of masses with inserted flux is proposed as an architecture for a qubit. This proposal is distinct from those coupling to superconductors¹⁹ and will be described in Sec. V.

II. SPECTRAL ASYMMETRY AND ANOMALY

This section is intended to review background material to be used in Secs. III and IV. The quantum anomaly can be understood and computed by two main routes. For a (2+1) dimensional Dirac theory on the infinite plane coupled to a background gauge field $A^\mu(x)$, one can simply compute the effective action and extract the current term^{9,10}

$$\begin{aligned} \langle j^\mu \rangle &= i \frac{\delta}{\delta A_\mu} \ln \det(i \not{D} + e \not{A} - m) \\ &= \frac{e^2}{8\pi} \frac{m}{|m|} \epsilon^{\mu\nu\lambda} F_{\nu\lambda} + \dots \end{aligned} \quad (1)$$

$$\therefore \langle Q \rangle = \int \langle j^0 \rangle = \frac{e}{2} \Phi$$

where the field strength $F_{\mu\nu} = \partial_\mu A_\nu - \partial_\nu A_\mu$ and $\Phi = -e \int d^2r B / (2\pi)$. While this gives an exact analytic result, explicit computation of the log of the determinant is difficult in all but the simplest cases such as the infinite plane.

An alternate route to understand the anomaly is more suited for the program of this paper. One can attempt to diagonalize the single particle Dirac Hamiltonian H , $H\psi_\lambda(\vec{x}) = E_\lambda\psi_\lambda(\vec{x})$. ψ 's are n -component classical spinors, H contains γ^μ matrices satisfying $\{\gamma^\mu(x), \gamma^\nu(x)\} = g^{\mu\nu}(x)$ and g is the coordinate metric (see Refs. 20 and 21 for more information). Then the fermion annihilation operator at \vec{x} can be expanded in this basis:²²

$$\Psi(\vec{x}) = \sum_o a_o \psi_o + \sum_{+\lambda} a_{+\lambda} \psi_{+\lambda}(\vec{x}) + \sum_{-\lambda} b_{-\lambda}^\dagger \psi_{-\lambda}(\vec{x}) \quad (2)$$

Where $\psi_{\pm\lambda}$ are the positive(negative) energy eigenstates, ψ_o are possible zero energy states, and a, b are fermionic annihilation operators satisfying the usual commutation relations (here and below, λ with no \pm qualifier is taken to mean *any* eigenstate). The sum/integral is shorthand to account for the fact that the spectrum may be partly discrete and partly continuous in open systems (this will just be taken to be a sum from now on). In applications with only bound states, or in closed systems, if the ψ_λ are normalized, then $\{\Psi^\dagger(\vec{y}), \Psi(\vec{x})\} = \delta^{(2)}(\vec{x} - \vec{y})$. Alternatively, continuum states can be chosen to satisfy this condition. The current operator which couples to the electromagnetic potential is the combination $J^\mu(\vec{x}) = \frac{-e}{2} (\Psi^\dagger(\vec{x}) \gamma^0 \gamma^\mu \Psi(\vec{x}) - (\Psi(\vec{x}))^{Ts} (\Psi^\dagger(\vec{x}) \gamma^0 \gamma^\mu)^{Ts})$. (The sum of different orderings is necessary to avoid an infinite constant coupling to the potential; it is also the properly transforming operator under charge conjugation.) In particular the charge operator is:

$$\begin{aligned} \frac{Q}{-e} &= \frac{1}{-e} \int J^0 = \sum_{\pm\lambda} (a_{+\lambda}^\dagger a_{+\lambda} - b_{-\lambda}^\dagger b_{-\lambda}) \\ &\quad + \sum_o a_o^\dagger a_o - \frac{1}{2} \eta \end{aligned} \quad (3)$$

where the spectral asymmetry is defined,

$$\eta \equiv \sum_{E_\lambda \geq 0} 1 - \sum_{E_\lambda < 0} 1. \quad (4)$$

Note that it is asymmetry between positive and negative spectra that lead to fractional charges. For continuum states the formula is not well defined as it needs to be regularized. To make contact with Eq. (1) and if one cares about the distribution of charge in the vacuum(a) (as we do below), then instead $\langle J^\mu(\vec{x}) \rangle$ may be computed. Taking the vacuum(a) to be all negative energies states filled (no holes), positive energy states unfilled and, if they exist, various zero-energy states occupied (defining the different vacua), the result for the charge density is:

$$\begin{aligned} \frac{1}{-e} \langle J^0(\vec{x}) \rangle &= -\frac{1}{2} \sum_{\pm\lambda} (|\psi_{+\lambda}(\vec{x})|^2 - |\psi_{-\lambda}(\vec{x})|^2) \\ &\quad + \frac{1}{2} \sum_o |\psi_o(\vec{x})|^2 - \frac{1}{2} \sum_u |\psi_u(\vec{x})|^2 \end{aligned} \quad (5)$$

and the current (with $\gamma = \gamma(\vec{x})$ and $\psi = \psi(\vec{x})$):

$$\begin{aligned} \frac{1}{-e} \langle J^i(\vec{x}) \rangle &= -\frac{1}{2} \sum_{\pm\lambda} (\psi_{+\lambda}^\dagger \gamma^0 \gamma^i \psi_{+\lambda} - \psi_{-\lambda}^\dagger \gamma^0 \gamma^i \psi_{-\lambda}) \\ &\quad + \frac{1}{2} \sum_o \psi_o^\dagger \gamma^0 \gamma^i \psi_o - \frac{1}{2} \sum_u \psi_u^\dagger \gamma^0 \gamma^i \psi_u \end{aligned} \quad (6)$$

where $\pm\lambda$ refers to non-zero states and o, u sum over occupied(unoccupied) zero modes. To extract the charge in one region versus another $\langle J^0(\vec{x}) \rangle$ may be integrated over regions of interest, as we shall do below. Formulae

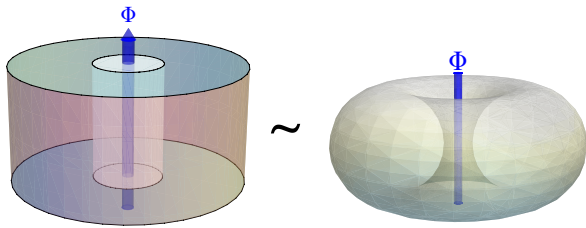


FIG. 1. (Color online) The pierced cylinder with threaded flux (left) is considered in Sec III idealized to a torus (right).

(5), (6) will be used below to compute various anomalous currents.

Before describing the present analysis, I will briefly describe the results of Jaroszewicz and Kiskis.^{23,24} They undertake the same program in the prototypical example of a B-field, $B(r)$, localized at the origin (r is the distance from the origin) piercing the 2D plane. In this case, if $\lim_{r \rightarrow \infty} B(r)r^2 \neq \infty$ then there will be continuum states which scatter off the localized B -field. If Φ (the total flux in units of $2\pi/e$) is non-integer, the spectral asymmetry of these continuum states (properly regularized) will contribute an amount equal to the non-integer part, while the existence of N localized states, $N \leq \Phi < N+1$, at $E = -m$ for $eB > 0$ or $E = m$ for $eB < 0$ also contribute with a value equal to the integer part in the spectral asymmetry. Note that unlike the one-dimensional fractional charge found by Jackiw and Rebbi,²² the 2-D case features a charge only algebraically localized. The closed cylinder cases treated below will feature a more complicated topology, but the spectrum will be discrete thereby making the analysis in terms of spectral asymmetry straightforward once the spectrum and wavefunctions are known.

III. FLAT TORUS: DEFORMED PIERCED CYLINDER

As discussed in the introduction, I first consider a simple example motivated by a hole drilled through a cylinder, which is smoothed out into a torus as shown in Fig. 1 and further idealized as the flat torus. The results will be useful to contrast with those of the next section and may also be relevant to a microscopically localized flux (to be discussed below).

Generically I will use coordinates z and ϕ for the two orthogonal directions on the torus. In these coordinates a flat metric can be used. Before writing down the Dirac equation, it is important to note that several inequivalent forms can be used on the torus. Writing the torus as a square with edges identified naturally leads one to a cartesian-like form (with constant Pauli matrices). However, this will not agree from an embedding in 3-dimensional Euclidian space as used in Refs. 17, 25, and

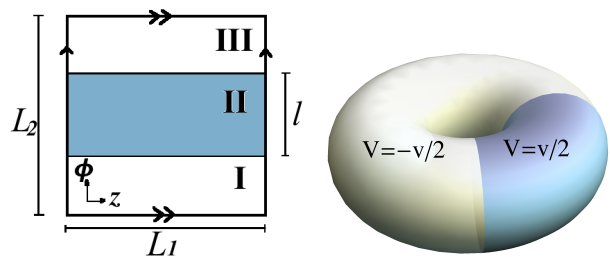


FIG. 2. (Color online) Coordinates and dimensions (left) for the smooth torus (right). Note sides are identified in the left figure. The surface is massive (constant) everywhere, but a non-zero scalar step-like potential is introduced with values as shown by V (right). z is in the vertical direction at right. Note the torus is separated into two regions, or three with edges identified, which will be labeled as I, II, III.

26. While both forms are mathematically consistent they lead to different physical results. The reason is that on the torus there are four spin structures, a pair for each fundamental loop. In general there are 2^{2g} spin-structures for a surface with g handles. They *are not* related by a spin-gauge transformation. The spectrum, for example, has a finite-size gap present depending on the spin-structure. However, none of the conclusions made here will crucially depend on this or the spin-structure choice. Therefore I will pick the spin structure that reproduces the half-integer azimuthal dependence found for the unique choice in the case of a *closed* (with caps) cylinder (see Sec. IV and the appendix). It is also the choice which leads to a derivation of the Dirac equation by embedding. Then, using coordinates like those in Fig. 2, the massless Dirac equation is (up to spin-gauge transformations):

$$e^{-i\frac{\sigma^3}{2}\phi}(-i\sigma^1\partial_z - i\sigma^2\partial_\phi)e^{i\frac{\sigma^3}{2}\phi}\psi_\alpha = E\psi_\alpha. \quad (7)$$

This equation is equivalent with the one found in Ref. 17, 25, and 26 for infinite cylinders if one makes a different identification of the gamma matrices γ^a , or equivalently makes the legitimate spin-gauge transformation of Eq. (7): $\psi \rightarrow \exp(i\frac{\sigma^3}{2}\phi) \left(\frac{1-i\sigma^2}{\sqrt{2}} \right) \exp(-i\frac{\sigma^3}{2}\phi)\psi$.

A. Anomalous Hall current; independence on mid-gap states

The first case I consider is the simplest situation to ascertain an anomalous Hall conductance as a function of mass-strength: a fully massive Dirac fermion (same-sign mass term throughout the surface) with a step potential in the $\hat{\phi}$ direction $V(\phi) = v(\Theta(\phi+l/2) - \Theta(\phi-l/2)) - v/2$, corresponding to localized electric field at $\pm l/2$, $\vec{E} = (-\delta(\phi+l/2) + \delta(\phi-l/2))v\hat{\phi}$. This is shown in Fig. 2. The units are set with $L_1 = 2\pi$ while other quantities are measured in units of L_1 , $L_2 \rightarrow 2\pi L_2/L_1$, $l \rightarrow 2\pi l/L_1$.

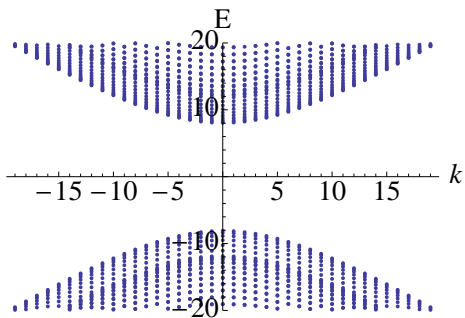


FIG. 3. (Color online) Sample spectrum for the case $m = 10$, $v = 4$, $l = 2$, $L_2 = 5$. Units are defined in the text.

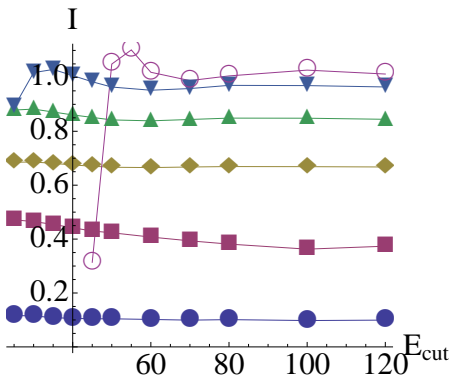


FIG. 4. (Color online) Hall current, I (in the \hat{z} -direction) in units of $-e/2v$ along a window (of width $= L_2/100$) around $\phi = -l/2$. The same result is obtained along the strip where $\phi = l/2$ with sign reversed. From infinite plane result, $I = 1$ expected. The x -axis labels the cutoff energy employed (that is all states below said energy are summed to approximate the delta function peak). Each line represents a different mass: from top to bottom $m = 40, 20, 10, 5, 2.5, .5$ (in units of $2\pi/L_1$). All cases take $v = 4$, $l = 2$, and $L_2 = 5$.

Then the Dirac equation is ($\gamma^0 = \sigma^3, \gamma^z = \sigma^3\sigma^1, \gamma^\phi = \sigma^3\sigma^2$):

$$e^{-i\frac{\sigma^3}{2}\phi}(-i\sigma^1\partial_z - i\sigma^2\partial_\phi + \sigma^3m - eV(\phi))e^{i\frac{\sigma^3}{2}\phi}\psi = E\psi. \quad (8)$$

with $0 \leq z < 2\pi$ and $-L_2/2 \leq \phi < L_2/2$ while mass and energy are normalized to units of $2\pi/L_1$. The solutions in each region involve a linear combination of two plane waves. The six matching conditions (two components at each boundary set equal to each other) and normalization determines all six coefficients plus the quantization condition (see appendix for details). The corresponding spectrum is shown in Fig. 6. The angular momentum in the \hat{z} direction, k , is a good quantum number and is integer-valued for the case of Eq. (8). Note the spectrum is fully gapped $\sim m$ even for any value of threaded flux (not shown).

Nevertheless the anomalous Hall current, $j^z(\phi)$, is non-zero and can be computed numerically using Eq. (6). Ac-

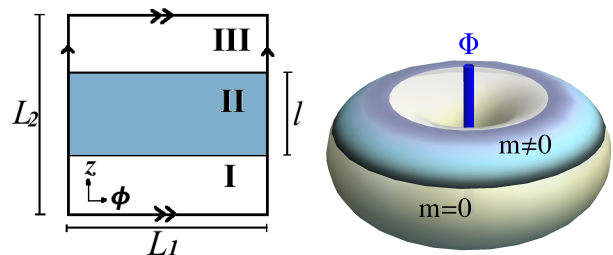


FIG. 5. (Color online) Coordinates and dimensions (left) for the smooth torus (right). Note sides are identified in the left figure and ϕ and z have been exchanged relative to Fig. 2. However, at right, z is still in the vertical direction. A mass term, m , is present only in the shaded area, region II. The torus is separated into two regions, or three with edges identified, as shown in at left labeled I, II, III.

cording to the infinite plane result, one expects $\frac{j^z(\phi)}{-e} = (\delta(\phi + l_\phi/2) - \delta(\phi - l_\phi/2))\frac{e}{2}\text{Sign}(m)$. The computed result turns out to have a smoother mass dependence. The computed values are summarized in Fig. 4. The figure shows the total current in the \hat{z} along a window (of width $= L_2/100$) localized at $\phi = -l/2$, as more and more energy states are summed making the numerical approximation of the expected delta function better and better. If a window around $\phi = l/2$ is chosen, one obtains the negative value of those in the figure, and if any other window is chosen there is no current. The current smoothly approaches zero as the mass approaches zero. The results agree with the expectation of the localized Hall current when the mass-distance is large enough $m \sim 20$ (in units of $2\pi/L_1$). There is no further dependence on the potential strength beyond the expected (linear) scaling. These values are observable for macroscopic crystals as mentioned in the discussion section below (Sec. VI). Finally, note that the system exhibits a current despite remaining fully gapped (including with flux threaded), in contrast to arguments presented in Ref. 17. The current is simply encoded in the wavefunctions. This is consistent with the interpretation of the anomaly as arising from the path integral measure as opposed to the action itself (the classical action has the spectral information).

B. Massless and partially massive surface

The second case which is easily solvable in this geometry is simply having a strip of mass m on the surface, but no potential, as a check that no charge is accumulated anywhere after a threaded flux cycle despite having an edge to the massive region. Although this is intuitive in retrospect, results are presented to contrast with the next section having a closed-cap cylinder. The coordinates are shown in Fig. 5. Note z and ϕ directions are exchanged relative to Fig. 2 but the same normalization $L_1 \equiv 2\pi, L_2 \rightarrow 2\pi L_2/L_1, l \rightarrow 2\pi l/L_1$ is employed.

For the three regions $\alpha = \{I, II, III\}$, with $m_\alpha =$

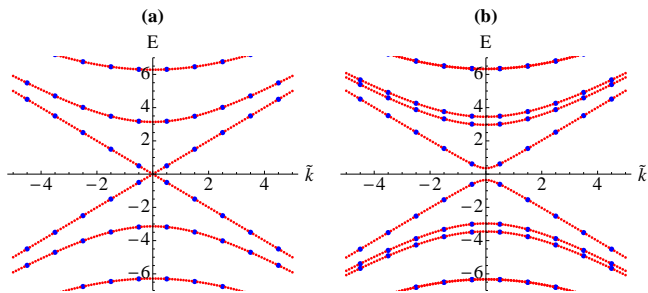


FIG. 6. (Color online) Massless case (a), $m = 0$ with $l = .5$ and $L_2 = 2$. (b) With mass $m = 1.5$, and same aspect ratios. The energy and mass are in units of $2\pi/L_1$. See text.

$\{0, m, 0\}$ the Hamiltonian is ($\gamma^0 = \sigma^3, \gamma^z = \sigma^3\sigma^1, \gamma^\phi = \sigma^3\sigma^2$):

$$e^{-i\frac{\sigma^3}{2}\phi}(-i\sigma^1\partial_z - i\sigma^2\partial_\phi + \sigma^3m_\alpha)e^{i\frac{\sigma^3}{2}\phi}\psi_\alpha = E\psi_\alpha. \quad (9)$$

The quantization condition derived in the appendix is solved numerically and the eigenvalues are shown in Fig. 6. The large(blue) points are at the allowed azimuthal quantum numbers $\tilde{k} \in \mathbb{Z} + 1/2$ of the wavefunction $\tilde{\psi}$ defined as $\tilde{\psi}_\alpha = e^{i\frac{\sigma^3}{2}\phi}\psi_\alpha$. Because of the half-integer quantization there is a finite-size energy gap, of order $1/L_2$. When a flux Φ is inserted its effect can be undone through a transformation which amounts to shifting $\tilde{k} \rightarrow \tilde{k} + \Phi$. Therefore the smaller(red) points show the evolution of the eigenvalues under this threaded flux. For the massless case (Fig. 6(a)), the bands traverse the gap. Of course in a pierced cylinder these bands simply reflect the fact that fermions could travel through the center around the torus.

As previously mentioned, these bands *are not* responsible for the Hall current and half-integer charge flow around the torus. In fact these bands simply result in a normal longitudinal conductivity as expected from band theory. After one unit of flux is threaded, the massless case develops a hole and occupied charge carrier through the $E = \pm k$ bands, but the wavefunction for these states are related by $\psi_{E \leq 0} = \sigma^3\psi_{E > 0} = \text{constant}$, and therefore in light of formulas (5) and (6) *no* net change in charge accumulates or current in the \hat{z} direction results. There is a constant current in the $\hat{\phi}$ direction $= 2\pi e^2$, which is the longitudinal current expected of free fermions accelerated under potential $2\pi e$.

For any small strip of mass, a gap forms for all fluxes as shown in Fig. 6(b). In this case the flow returns the vacuum to itself, and no charge accumulation is seen. The system behaves as though a mass were present globally and no edge exists. It can be proven that there is gap generated no matter how small the mass-strip size is, although numerically it can be shown that the gap dependence on the geometry is $\Delta \sim \text{Min}[1/(L_2 - l), m]$. This spectral flow is to be contrasted with the results of the next section. What is left unchecked is whether the gap generated by the strip induces the Hall current

with a potential explicitly present as done in the previous section.

IV. SURFACE OF A CLOSED CYLINDER

The more interesting case is the potential accumulation of fractional charge where magnetic fluxes penetrates the surface. It was argued in Ref. 17 that in fact surface electrons will tunnel through the bulk of a topological insulator for a very localized flux or if a hole is bored through the material. This was called the wormhole effect. Nevertheless, as argued below, I will consider it an open question, as to whether this effect would still manifest itself in a more diffuse flux.

A. Discussion on the wormhole effect and fidelity of surface theory

In light of the results of Sec. IIIB one notices similarities and differences with the result of Ref. 17. While I considered a smooth case, with finite-size gap $1/L_2$ it is clear such a gap will be of order $1/R$ where R is the radius of the interior of a bored cylinder. In this case, the effect of inserting a flux tube through a bored hole or a single plaquette of the microscopic lattice, can be removed by simply shifting the azimuthal number. The spectral flow will be similar to Fig. 6(a). For a flux that approximately permeates a single plaquette, indeed, these mid-gap states would correspond to a metallic bulk and the wormhole effect. However, these mid-gap states do not transmit anomalous current as previously discussed. In fact, band theory alone cannot explain the anomalous current.

A similar picture will result any time a simple global transformation can remove the effect of a threaded flux as when it goes through a hole or single plaquette. Thus the following ansatz is proposed: if an extremely localized flux string manages to pierce a single or a few plaquettes throughout the bulk, then the surface is equivalent to a genus one cylinder with a hole through it as in Fig. 7(a), since in this case both for the lattice and continuum theory the flux simply shifts the azimuthal number. In this case, just the surface theory of the torus spectrum contains the information (closing gap) corresponding to the ability for electrons to propagate through the interior surface of the torus. If instead the flux is smoothly varying and extended over many plaquettes, then it is still reasonable to expect the low energy theory on the surface be described faithfully by the Dirac theory on a closed cylinder i.e. surface of genus zero (this is illustrated in Fig. 7(b)). In this case it turns out that the physical inclusion of the flux in the manifold matters beyond simply shifting the azimuthal angle, and a fractional localized charge might be observed.

I will not investigate this potential crossover numerically but wish to present the surface theory results as-

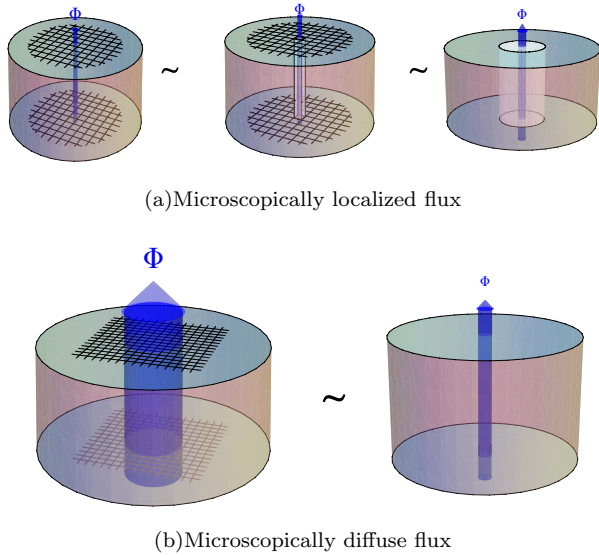


FIG. 7. (Color online) Contrasting a microscopically localized flux (a) as qualitatively equivalent to the genus one surface discussed in Sec. III B, with a diffuse flux which remains described by a surface theory of genus zero and penetrating flux (b). See text.

suming the ansatz to be correct. Whether or not it turns out to be true, it is still interesting to see the manifestation of the anomaly by solving the Dirac equation on the surfaces. In the intermediate regime where the flux is much larger than the lattice spacing, but still of a few inverse kelvin in length, the potential for qubit states might be an interesting application described in Sec. V.

B. Closed cylinder results

Motivated by a microscopically diffuse magnetic field applied to a solid cylinder I consider the Dirac theory on the surface of a cylinder with caps, as a potential construct to observe fractional charge accumulation (when various mass terms are present). The relevant dimensions and coordinates are described in Fig. 8. The Dirac equation in the three different sections and matching conditions are derived in the appendix, they are on the top and bottom caps:

$$\{(\sigma^1 \cos \phi + \sigma^2 \sin \phi) \partial_r + (\sigma^2 \cos \phi - \sigma^1 \sin \phi) \frac{\partial \phi}{r} + m_{\text{I,III}} \sigma^3\} \psi_{\text{I,III}} = E \psi_{\text{I,III}}(r, \phi) \quad (10)$$

and on the side:

$$e^{-i \frac{\sigma^3}{2} \phi} (-i \sigma^1 \partial_z - i \sigma^2 \partial_\phi + \sigma^3 m_{\text{II}}) e^{i \frac{\sigma^3}{2} \phi} \psi_{\text{II}} = E \psi_{\text{II}}(z, \phi), \quad (11)$$

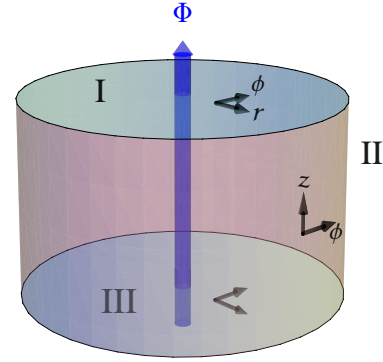


FIG. 8. (Color online) Closed cylinder of radius R , and side (cap-to-cap) length d . Three separate sections are labeled I, II, and III each with local coordinates as shown. The caps, I and III, have local polar coordinates with $\hat{r} \times \hat{\phi}$ oriented upward. The side has \hat{z} oriented in the upward direction, and the origin will be set in the center of the side. $\hat{\phi}$ globally has the same orientation. Different cases are considered where each section may separately have a constant oriented mass m_α . See text.

or defining in each region $\tilde{\psi} = \exp(i \frac{\sigma^3}{2} \phi) \psi$,

$$\begin{aligned} \left(-i \sigma^1 \partial_r - i \sigma^2 \frac{\partial \phi}{r} - \frac{i \sigma^1}{2r} + m_{\text{I,III}} \sigma^3 \right) \tilde{\psi}_{\text{I,III}} &= E \tilde{\psi}_{\text{I,III}} \\ (-i \sigma^1 \partial_z - i \sigma^2 \partial_\phi + m_{\text{II}} \sigma^3) \tilde{\psi}_{\text{II}} &= E \tilde{\psi}_{\text{II}} \end{aligned} \quad (12)$$

The matching conditions are:

$$\tilde{\psi}_{\text{I}}|_{r=R} = \sigma^2 \tilde{\psi}_{\text{II}}|_{z=d/2}, \quad \tilde{\psi}_{\text{III}}|_{r=R} = \tilde{\psi}_{\text{II}}|_{z=-d/2}. \quad (13)$$

The matching conditions themselves are more carefully derived in the appendix by smoothing out the corners and checking that spin connection term actually vanishes in the $\tilde{\psi}$ basis with no further transformation. Note as before the angular quantum number \tilde{k} of $\tilde{\psi}$ takes on *half-integer* values. I will consider six cases ($m > 0 \neq m(x)$): (a) massless case, $m_{\text{I}} = m_{\text{II}} = m_{\text{III}} = 0$ (b) positive mass on top cap alone $m_{\text{I}} = m$, $m_{\text{II}} = m_{\text{III}} = 0$, (c) positive mass on the side $m_{\text{II}} = -m$, $m_{\text{I}} = m_{\text{III}} = 0$ (d) positive mass on top and bottom $m_{\text{I}} = -m_{\text{III}} = m$, (e) positive mass everywhere $m_{\text{I}} = -m_{\text{II}} = -m_{\text{III}} = m$, and finally oppositely oriented masses on the two caps (f) $m_{\text{I}} = +m_{\text{III}} = m$, $m_{\text{II}} = 0$. Note the relative minus sign between the top and the rest of the cylinder in the cases (b)-(e) to describe a *same* sign mass, comes from the σ^2 transformation in the top-to-side matching stemming from the opposite orientation of the r and z directions at the top-side boundary.

Unlike the torus, the effect of the flux is not simply to shift the azimuthal quantum number. In particular some boundary condition must be implemented at the origin which physically involves the flux details. Interestingly a

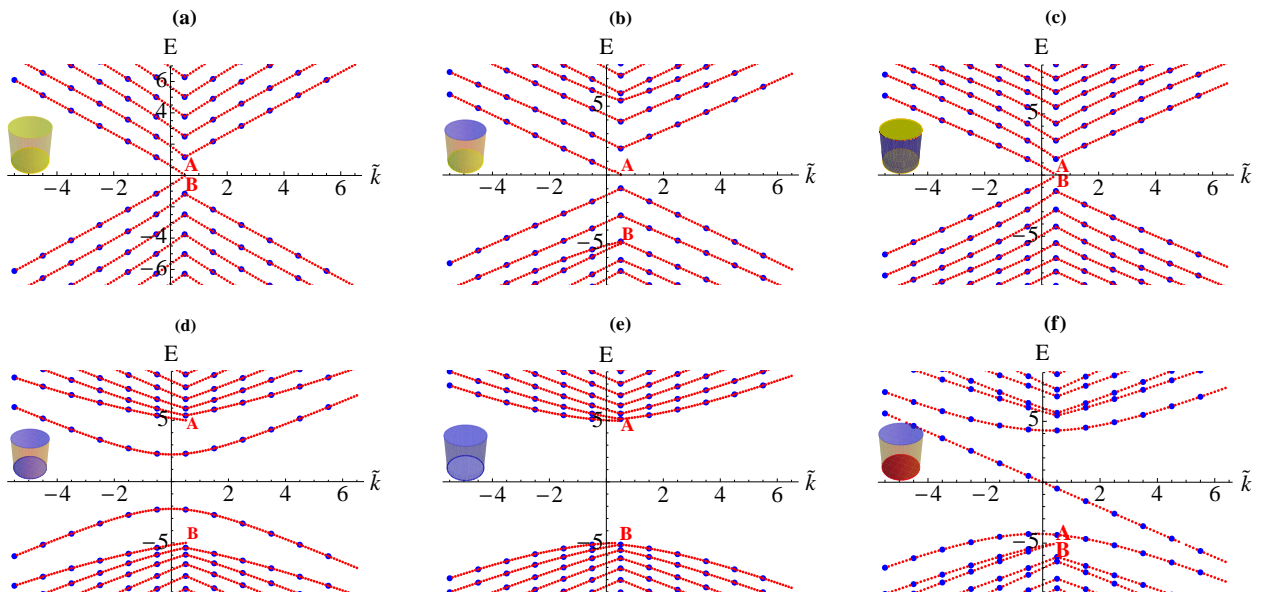


FIG. 9. (Color online) The spectra corresponding to the cases (a) through (f) defined in the text. Blue points at half-integer azimuthal number \tilde{k} are the spectra with no flux inserted. The red points represent the spectral flow as a localized flux is inserted as described in the text and shown in Fig. 8. After one unit of flux, new states appear at marked points A and B. The inset reproduces cylinders for each case with color scheme: yellow for the massless regions, blue for positive mass, and in the case of (f), red for a negative orientated mass. For all cases $|m|R = 5$, $d/R = 1/2$, and the energy is in units of $1/R$.

simple shift alone of \tilde{k} would allow for extra solutions, unconstrained by normalizability at the origin (see appendix and discussion in Refs. 18 and 27). This is fixed when the form of the flux is considered. The easiest situation is to take a profile for the flux as a localized delta-function-ring with small radius $B(r) = \Phi\delta(r-\epsilon)/(2\pi\epsilon)$.²⁷ This is just a theoretical approximation which is expected to be qualitatively similar to a diffuse flux of width ϵ . Figure 9 shows the spectrum for the different cases as a function of azimuthal quantum number \tilde{k} . As before, the large (blue) points represent the spectra with no flux, and the smaller (red) points are the evolution of the spectra as one unit of flux is inserted.

The effect of the flux is manifested by the appearance of extra states at the end of the cycle inserting one unit of flux. The extra states are shown where red (smaller) dots terminate at points where there was not a corresponding state previously or there are now two states where there was only one (initial states are in blue or larger dots). These are marked at the locations A and B in the figure for each case. As mentioned in Sec. II, the creation of new states relative to the original vacuum will have a half charge associated with them. For all cases a simple pattern emerges: “anomalous” bands create an extra state near $-m_I$ and m_{III} (A and B points). One can show that the states are never exactly at those values, including $E = 0$ for the massless case. All other bands flow back to, or very near, the original spectrum. The difference between the cases occurs in the relative distribution of the wavefunctions. Assuming negative energies are occupied one can consider what happens as the flux

is ramped to one unit. In case (a), the two states that appear near $E = 0$ each have a probability that is equally split between the top and bottom solenoid, so that no net charge-density appears accumulated, and as expected the conclusion is that no charge is pumped for the completely massless case. For cases (b)-(e), the new states are unevenly localized, and in particular the negative energy states are localized around the bottom cap flux while the positive on the top. As derived in the appendix, the functional dependence of the solution on the caps for these states are: $Y_{-1}(\sqrt{E^2 - m_{\text{cap}}^2})$ for $\Phi = 1$ and more generally for other integer Φ , $Y_{-\Phi}(\sqrt{E^2 - m_{\text{cap}}^2})$ (Y are Bessel functions of the second kind). Because $|E| > |m|$ (the energies are never exactly at m) for all the bands, the Bessel functions scale as $\sim \frac{1}{r^\Phi}$, and are therefore only algebraically localized, as in the infinite plane case.^{23,24} Although in the infinite plane for $\Phi = 1$ one solution is not allowed due to normalizability at infinity, while in this case they are allowed due to the closed nature of the surface. If the solenoid could pierce only one cap (a net outward flux), then a single $E = \pm m$ (with m the mass of that cap with flux) state would be found for $\Phi = 1$ in agreement with Index Theorems (see references within Refs. 9 and 28). In this case the pair of new states ensure the overall system remains neutral but the relative distribution of charge does not remain uniform.

Similar to the result of the torus, the mass dependence is not a perfectly quantized step function as in the infinite plane. Instead one can numerically calculate finite size

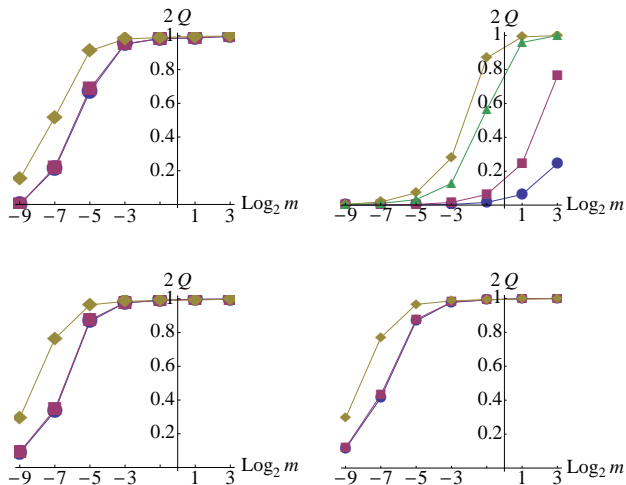


FIG. 10. (Color online) The total charge $\times 2$ (Q in units of $-e/2$) in the top cap after one unit of flux is inserted. Cases (b) through (e) clockwise, (b) starting at top-left. The horizontal axis plots a log scale of m which is physically mR since units are normalized by R . The various lines are for ratios $d/R = 1/32, 1/8, 2$ for the circle(blue), square(purple), and diamond(yellow) respectively. The side-mass case also has $d/R = 1$ shown in triangle(green).

effects in units of mass-radius, mR , for different aspect ratios d/R . The robustness of the quantization depends on the geometry of the masses. Figure 10 summarizes the results by showing the charge pumped into the top cap for different ratios d/R and mass-radii, mR , for cases (b)-(e). Generically the main contribution comes from the induced state which is localized. As a check, eigenstates up to $|E| = 30$, are also summed however there is little, if any, contribution from these; especially from the higher energies.

Finally the spectrum for case (f), continues with pattern of the anomalous bands, but now both of them appear at $E = -|m|$. Both of these states represent half-charge at each cap relative to the flux-less vacuum. Meanwhile the appearance of a chiral band is responsible for the appearance of an anti-charge localized on the massless side. Therefore the flow in this case ends with deficit fractional charges from the cap explicitly pumped to the sides.

V. QUBIT ARCHITECTURE

The pattern of the results from the previous section imply that unit fluxes induce new states with energy equal to the local mass. With this in mind it is possible to conceive of a configuration that will produce close to degenerate $E = 0$ states separated by an arbitrary energy gap. Before delving into describing specific magnitudes, I will describe the basic configuration in principle. Note this proposal is distinct to that of Ref. 19 involving Ma-

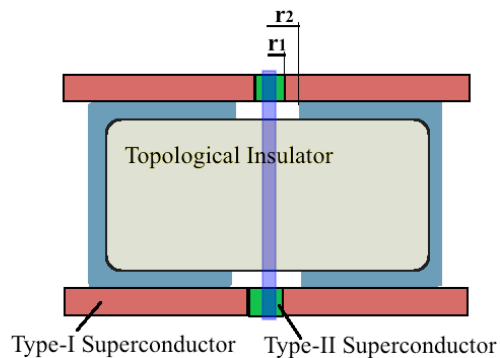


FIG. 11. (Color online) Cross-section of a configuration supporting a qubit. The blue band represents a ferromagnetic mass. See text for detailed explanation.

jorana fermions. The construction I will outline is shown in Fig. 11, however most of the details will be discussed further below. The basic idea is to imagine the cylinder coated with mass almost entirely (shown in blue around the topological insulator surface) except for a region of radius r_2 . If $r_2 \sim 1/m$ then any state localized in r_2 will be gapped by order m as well, thereby making the entire spectrum gapped by m . Now if a localized flux can be inserted within r_2 , with width of say r_1 , it will induce a low energy state which in the limit of an ultra-localized flux will approach $E = 0$ (note there will be two such states corresponding to the top and bottom windows).

While in previous sections I have been considering a single unit of flux. When more than one unit of flux is inserted, other states which start at lower \tilde{k} flow down into the gap towards $E=0$. The flow is along the same, or similar, trajectory. A generic picture is that of Fig. 12 which shows the flow of energy states as up to two units of flux are inserted. Specifically, after two units of flux, then relative to the original spectrum, there will be a new pair of states with $E \sim \pm 0$ at $\tilde{k} = 3/2$, and a new pair at $\tilde{k} = 1/2$, while the rest of the spectrum remains at $|E| \geq \sim m$. If a third unit of flux were inserted there would be three pairs, etc. Furthermore, as in case (c) of the previous section, each of these states will be localized in different regions: $E \sim +0$ states will be localized in the bottom flux-piercing while $E \sim -0$ states will be on top. Therefore $E > 0$ and $E < 0$ states will not be mixed by local noise (different \tilde{k} states however can be). If, however, the flux is fractional there will in general be one state in the mid-gap region spoiling the energy separation. These would lie in the intermediate region along the line between $\tilde{k} = -1/2$ and $1/2$ in Fig. 12. Therefore a limiting factor is the need for integer flux. A second issue, is that for the energies to flow to a value sufficiently close to $E = 0$, r_1 , the flux width, must be sufficiently small compared to r_2 , otherwise the mass exerts a proximity effect for the $\tilde{k} = 1/2$ state. The induced state for four different radii r_1 are shown in Fig. 12. From the figure, at least $r_1 < .1r_2$ is required for reasonable energy scale separation.

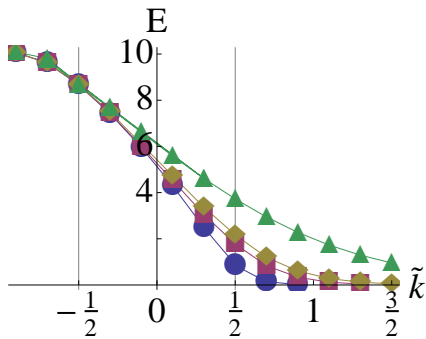


FIG. 12. (Color Online) The energies of the induced state as a localized flux is inserted for the configuration of Fig. 11. Up to two units of flux are shown. Note that symmetric $E < 0$ states are not shown. States starting at $\tilde{k} = -1/2$ flow to $\tilde{k} = 3/2$, while a second state starting from $\tilde{k} = -3/2$ flows to $\tilde{k} = 1/2$ along a similar curve. The four curves from top to bottom represent more localized fluxes with $r_1 = .5r_2, .1r_2, .05r_2, .001r_2$ respectively. All cases have $r_2 = .1R$ and $m = 10 R^{-1}$. Other states that are not shown have energies $|E| \sim 10$ as in Fig. 13. See Sec. VI for discussion on magnitudes.

Finally requiring a small r_1 and integer flux, are still not sufficient. Consider the spectrum for two units of flux inserted. Approximating the near-zero energies as being zero, the non-interacting many-body system exhibits approximate vacua gotten by re-arranging the occupation of the $E \sim 0$ states. Starting from a mid-gap fermi energy with no flux and inserting two units of flux would naively lead to a vacuum of two occupied $E \sim 0^-$ states. However, because these states are localized in r_1 (which is assumed small), the Coulombic interaction of electron would become strong. With the interactions turned on, this state is actually much higher in energy than the other 4 states having one $E < 0$ state occupied and one $E > 0$ occupied, which are net neutral in the r_1 windows. For odd flux the system would prefer to have just a single unpaired occupied state as its lowest energy configuration and therefore have a fractional half charge at each window (there is no completely neutral configuration in this case). Because it is most feasible to have a qubit system distinguished by charge, the odd flux then becomes a requirement as well, which requires precision up to a single flux quantum (since fluctuation through an even number would destroy the charge and presumably control). For practical purposes, this amounts to requiring a single flux quantum pierce the cylinder along the windows.

Still all these constraints may have a potential solution. To shield flux from regions where it is not wanted, a (type-I) superconductor can be put over the top and bottom surfaces as shown (Fig. 11) with holes of radius r_1 . The induced current of the superconductor would favor integer flux through r_1 , which because it is small could easily be accommodated by a reasonable macroscopic magnetic field over the whole cap. However to further stabilize the single flux constraint, a Type-II su-

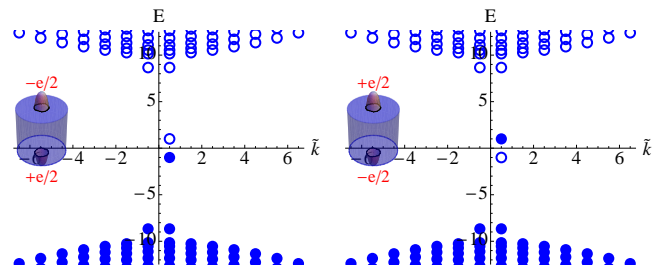


FIG. 13. (Color Online) Electron occupation (filled points) and insets showing charge density (plotted on the surfaces) for qubit states $|1\rangle$ (left) and $|2\rangle$ (right). Solutions are for the same parameters as those in Fig. 12.

perconductor could be used with the temperature of the system tuned so that the vortex coherence length $\sim r_1$ favoring a single vortex. Other possibilities perhaps using SQUIDS might also be suited.

If a single flux quantum can be stabilized then the basis of the qubit are simply the occupation of $E \sim 0^{(+)-}$ state, as shown in Fig. 13, $|1\rangle = a_{0-}^\dagger \left(\prod_{E \leq m} b_E^\dagger \right) |0\rangle$, $|2\rangle = a_{0+}^\dagger \left(\prod_{E \leq m} b_E^\dagger \right) |0\rangle$ (in the convention of Sec. II). $|1\rangle$ has a $-e/2$ charge at the top window ($+e/2$ at bottom) and vice versa for $|2\rangle$. Then in this basis, applying an electric field, or a potential V with $V|_{\text{top}} = -V|_{\text{bottom}} = v$, generates a term in the Hamiltonian $\sim v\sigma^3$ in the qubit subspace. A σ^1 or σ^2 matrix element necessary for full unitary evolution, is less trivial. Effectively switching the electron occupation is required. One potential route is simply inserting metallic electrodes connecting the top and bottom windows, allowing the electron to tunnel and with the aid of a bias voltage. The technicalities of this route and other possibilities, however, are left for future work.

VI. MAGNITUDES AND DISCUSSION

In summary the details of how anomalous currents manifest themselves on the surface of topological insulators has been presented. Most striking is the finite-size scaling which is exhibited in these more realistic geometries. This result also makes more sense physically than the sharp $\text{Sign}(m)$ dependences found for the infinite plane. Also the source of anomalous currents has been clarified: in the genus one topology flux threading modified the eigenfunctions but not the eigenspectra in any appreciable way, while inserting fluxes which pierce the surface creates new low lying states responsible for charge accumulation.

It was noted for the torus that $mL/2\pi \sim 20$ was necessary for the onset of full quantization while for the closed cap geometry, from Fig. 10, onset occurs at $mR \sim 1/8$ for massive caps and $md \sim 8$ for mass on the sides of the cylinder (case c). For a typical Fermi velocity⁶⁻⁸ $v_f = 10^6$ m/s, setting L , d , or R on order of 1 mm would

correspond to $m = 8 \times 10^{-2}$, 5×10^{-3} , 8×10^{-5} meV respectively, or for L , d , R of order $1 \mu\text{m}$, full quantization begins at $m = 80$, 5 and 8×10^{-2} meV. These are well within experimentally observed time-reversal breaking surface mass terms of order meV.¹⁶ The wide range of values suggests that the effect is strongly geometry dependent, and as such these values should only be taken as rough guides.

The required magnitudes for the qubit proposal is more constraining. Using the value for v_f above, for a gap of $3^\circ\text{k} \sim .3$ meV, a value of $r_2 = 2.5 \mu\text{m}$ is required. Therefore $r_1 \lesssim .1 \mu\text{m}$, which is small. The value of R and the aspect ratio is essentially unconstrained.

Finally, whether the fractional charge remains intact for a diffuse enough magnetic field remains an open question which can be investigated both numerically and experimentally.

VII. ACKNOWLEDGMENTS

This research was originally stimulated by discussions with Dung-Hai Lee. I also greatly benefited from many

useful and stimulating discussions with Jörg Gramich.

Appendix A: Wavefunctions and quantization condition on the torus

Although it is simple enough to write the Dirac equation and the form of solutions for both of the cases in the text, in order to not clutter up the notation I will split them. For a review on vielbeins and spinors in curved space see Refs. 21, 29, and 30.

1. Case 1: Fully massive torus; step potential in $\hat{\phi}$ direction

As discussed in the text (with unit definitions), for a fully massive torus with a potential $V_\alpha = (-v, +v, -v)$ for regions I, II, III as in Fig. 2 the Dirac equation is:

$$(-i\sigma^1\partial_z - i\sigma^2\partial_\phi + \sigma^3m)\tilde{\psi}_\alpha = (E - V_\alpha)\tilde{\psi}_\alpha \quad (\text{A1})$$

To simplify the formulae I've put v instead of $-ev/2$. In this case the \hat{z} direction is trivial and solutions are of the form $\tilde{\psi} = \exp(ikz)f_\alpha(\phi)$ with $k \in \mathbb{Z}$ (the same k in all regions). If $E \neq \pm\sqrt{k^2 + m^2} \pm v$ and $E \neq \pm|k|$, $f_\alpha(\phi)$ is given by:

$$f(\phi) = A_\alpha \left(\frac{1}{i\sqrt{(E-V_\alpha)^2 - k^2 - m^2} + k} \right) e^{i\sqrt{(E-V_\alpha)^2 - k^2 - m^2}\phi} + B_\alpha \left(\frac{1}{-i\sqrt{(E-V_\alpha)^2 - k^2 - m^2} + k} \right) e^{-i\sqrt{(E-V_\alpha)^2 - k^2 - m^2}\phi} \quad (\text{A2})$$

The coefficients in each region and energy quantization are determined by normalization and matching conditions $f_{\text{I}}(L_2/2) = \eta f_{\text{III}}(-L_2/2)$, $f_{\text{I}}(l/2) = f_{\text{II}}(l/2)$ and $f_{\text{III}}(-l/2) = f_{\text{II}}(-l/2)$ with $\eta = -1$ for the chosen spin-structure in the $\hat{\phi}$ direction. The quantization condition is:

$$\begin{aligned} |a|^2(\cos(pl + q(L_2 - l)) - 1) = \\ |b|^2(\cos(pl - q(L_2 - l)) - 1) \end{aligned} \quad (\text{A3})$$

where I have defined $q = \sqrt{(E+v)^2 - k^2 - m^2}$, $p = \sqrt{(E-v)^2 - k^2 - m^2}$, $a = \frac{k+ip}{E-v+m} - \frac{k-iq}{E+v}$, and $b = \frac{k+ip}{E-v+m} - \frac{k+iq}{E+v}$. This is solved numerically and shown (for a representative case) in Fig. 4. The special cases $E \neq \pm\sqrt{k^2 + m^2} \pm v$ and $E \neq \pm|k|$ (and special sub-cases of these such as $E = 0$) must be treated separately

although in a similar manner as above. The solutions in those cases are linear in one of the regions, and in general do not yield new solutions.

2. Case 2: Partially massive strip

In this case the Dirac equation is:

$$(-i\sigma^1\partial_z - i\sigma^2\partial_\phi + \sigma^3m_\alpha)\tilde{\psi}_\alpha = E\tilde{\psi}_\alpha \quad (\text{A4})$$

where $m_\alpha = (0, m, 0)$ for regions I, II, III as in Fig. 5. Different spin-structures are encoded in whether the boundary condition on $\tilde{\psi}$ is anti-periodic or periodic in ϕ . In each region I, II, III the solutions are of the form $\tilde{\psi} = \exp(i\tilde{k}\phi)f(z)$ with $\tilde{k} \in \mathbb{Z} + 1/2$. If $E \neq \pm\sqrt{\tilde{k}^2 + m^2}$ and $E \neq \pm|\tilde{k}|$, $f(z)$ is given by:

$$f(z) = A \left(\frac{1}{\sqrt{E^2 - \tilde{k}^2 - m^2} + i\tilde{k}} \right) e^{i\sqrt{E^2 - \tilde{k}^2 - m^2}z} + B \left(\frac{1}{-\sqrt{E^2 - \tilde{k}^2 - m^2} + i\tilde{k}} \right) e^{-i\sqrt{E^2 - \tilde{k}^2 - m^2}z}. \quad (\text{A5})$$

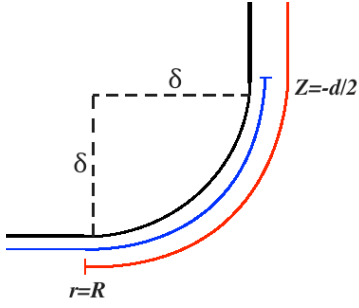


FIG. 14. (Color online) Side view of smoothed out cylinder edge.

where the region label has been omitted and the mass m is understood to be zero in region I and III. The coefficients in each region and energy quantization are determined by normalization and matching conditions $f_{\text{I}}(L_2/2) = \eta f_{\text{III}}(-L_2/2)$, $f_{\text{I}}(l/2) = f_{\text{II}}(l/2)$ and $f_{\text{III}}(-l/2) = f_{\text{II}}(-l/2)$ with $\eta = 1$ for the chosen spin-structure along \hat{z} loops. The quantization condition is similarly:

$$|a|^2 \cos(pl + q(L_2 - l)) = |b|^2 \cos(pl - q(L_2 - l)) \quad (\text{A6})$$

but in this case the definitions are $q = \sqrt{E^2 - \tilde{k}^2}$, $p = \sqrt{E^2 - \tilde{k}^2 - m^2}$, $a = \frac{\tilde{k} + ip}{E + m} - \frac{\tilde{k} - iq}{E}$, and $b = \frac{\tilde{k} + ip}{E + m} - \frac{\tilde{k} + iq}{E}$. This is solved numerically and shown (for a representative case) in Fig. 6. The special cases $E = \pm\sqrt{\tilde{k}^2 + m^2}$ and $E = \pm|\tilde{k}|$ (and special sub-cases of these such as $E = 0$) must be treated separately although in a similar manner as above. The solutions in those cases in general do not yield new solutions.

Appendix B: Dirac equation on closed cylinder surface

In the notation of Fig. 8, the closed cylinder is divided into three regions. The local form on the caps is as the Dirac equation for the disk described in Eq. 10 which can be gotten by transforming the Dirac equation in cartesian coordinates into polar coordinates (see Ref. 18 however a potential pitfall using vielbeins). For a review on vielbeins and spinors in curved space see Refs. 21, 29, and 30. To guess the form on side, region II, one cannot simply replace $r \rightarrow R$ as the metric suggests. In particular the spin connection is wrong, and stems from the fact that all the curvature is at the sharp corner where the coordinate transformation is required. A real manifold must be smooth and the transition between charts should be a map between $\mathbb{R}^2 \rightarrow \mathbb{R}^2$,

although in practice one dimension can be made of infinitesimal width if the manifold is smooth. This suggests a more careful procedure is to smooth the corners into a semi-circle of radius δ as in Fig. 14. Replacing the relation $\delta^2 = (r - R)^2 + (z + \frac{d}{2})^2$ into the 3-dimensional Cartesian metric, the induced metric is,

$$g = -\frac{\delta^2}{\delta^2 - (r - R)^2} dr \otimes dr - r^2 d\phi \otimes d\phi \quad (\text{B1})$$

and leads to the Dirac equation (using ϕ dependent vielbeins; see Ref. 18) in (r, ϕ) :

$$e^{-i\frac{\sigma^3}{2}\phi} \left\{ -i\sigma^1 \frac{\sqrt{\delta^2 - (r - R)^2}}{\delta} \partial_r - i\sigma^2 \frac{\partial_\phi}{r} - i\sigma^1 \frac{\sqrt{\delta^2 - (r - R)^2}}{2\delta r} \right\} e^{i\frac{\sigma^3}{2}\phi} \psi = E\psi. \quad (\text{B2})$$

As $r \rightarrow R$, the equation becomes

$$e^{-i\frac{\sigma^3}{2}\phi} \left\{ -i\sigma^1 \partial_r - i\sigma^2 \frac{\partial_\phi}{R} - \frac{i\sigma^1}{2R} \right\} e^{i\frac{\sigma^3}{2}\phi} \psi = E\psi, \quad (\text{B3})$$

just what we expect on the cap evaluated at $r = R$. However, replacing $r(z)$ and taking $z \rightarrow \frac{-d}{2}$ one gets:

$$e^{-i\frac{\sigma^3}{2}\phi} \left\{ -i\sigma^1 \partial_z - i\sigma^2 \frac{\partial_\phi}{R + \delta} \right\} e^{i\frac{\sigma^3}{2}\phi} \psi = E\psi, \quad (\text{B4})$$

just what one expects from the side using an embedding, without any further transformation of ψ i. e. $\tilde{\psi}_{\text{III}}(R, \phi) = \tilde{\psi}_{\text{II}}(-d/2, \phi)$. Less trivially is the boundary condition between the top and the side. The derivation proceeds in the same way if the local \hat{z} were facing down. So if one defines a new $z_n = -z$, and calls the tentative wavefunction $\psi_{\text{II}n}$ with the notation $\tilde{\psi}_{\text{II}n} = e^{i\frac{\sigma^3}{2}\phi} \psi_{\text{II}n}$ one would have found $(-i\sigma^1 \partial_{z_n} - i\sigma^2 \frac{\partial_\phi}{R}) \tilde{\psi}_{\text{II}n}(z_n, \phi) = E \tilde{\psi}_{\text{II}n}(z_n, \phi)$ (with boundary condition $\tilde{\psi}_{\text{I}}|_{r=R} = \tilde{\psi}_{\text{II}n}|_{z=d/2}$) which is $(+i\sigma^1 \partial_z - i\sigma^2 \frac{\partial_\phi}{R}) \tilde{\psi}_{\text{II}n}(z, \phi) = E \tilde{\psi}_{\text{II}n}(z, \phi)$. Evidently, then, the new $\psi_{\text{II}n} = \sigma^2 \tilde{\psi}_{\text{II}}$, since $\sigma^2 \sigma^1 \sigma^2 = -\sigma^1$.

In summary Eqs. 12 and 13 are obtained.

Appendix C: Wavefunctions and quantization condition on cylinder

The local solutions to Eq. 12 (if there is no flux) are for the caps $\tilde{\psi}_{\text{I,III}} = \exp(i\tilde{k}\phi) f_{\text{I,III}}(r)$. If $E \neq \pm\sqrt{\tilde{k}^2 + m_{\text{I,III}}^2}$ and $E \neq \pm m_{\text{I,III}}$, $f(r)$ has the form:

$$f(r) = C_1 \left(\frac{J_{\tilde{k}-\frac{1}{2}}(\sqrt{E^2 - m^2}r)}{i\sqrt{E^2 - m^2} J_{\tilde{k}+\frac{1}{2}}(\sqrt{E^2 - m^2}r)} \right) + C_2 \left(\frac{Y_{\tilde{k}-\frac{1}{2}}(\sqrt{E^2 - m^2}r)}{i\sqrt{E^2 - m^2} Y_{\tilde{k}+\frac{1}{2}}(\sqrt{E^2 - m^2}r)} \right) \quad (\text{C1})$$

where a region label =I, III should be understood for the mass m , $f(r)$ and the coefficients C_1 and C_2 . $\tilde{k} \in \mathbb{Z} + 1/2$ is globally the same value for all regions, and different \tilde{k} are linearly independent as required from the boundary condition along the ϕ direction (they are good

quantum numbers). $J_n(r)$, $Y_n(r)$ are Bessel functions, the two independent solutions satisfying $r^2 \frac{d^2 h}{dr^2} + r \frac{dh}{dr} + (r^2 - n^2)h = 0$, $J, Y = h(r)$ ($J_n(r)$ and $J_{-n}(r)$ also work if n is not an integer). The solution on the side is $\tilde{\psi}_{\text{II}} = \exp(i\tilde{k}\phi)f_{\text{II}}(r)$, and if $E \neq \pm\sqrt{\tilde{k}^2 + m_{\text{II}}^2}$ and $E \neq \pm m_{\text{II}}$, $f(r)$ is (again omitting region II label):

$$f(z) = A \left(\frac{1}{\sqrt{E^2 - \tilde{k}^2 - m^2 + i\tilde{k}}} \right) e^{i\sqrt{E^2 - \tilde{k}^2 - m^2}z} + B \left(\frac{1}{-\sqrt{E^2 - \tilde{k}^2 - m^2 + i\tilde{k}}} \right) e^{-i\sqrt{E^2 - \tilde{k}^2 - m^2}z}. \quad (\text{C2})$$

Square-integrability at the origin sets one of the coefficients of the cap to zero, when $|\tilde{k}| \geq 1/2$. Using the boundary conditions discussed in the previous section, the remaining coefficients are determined along with the quantization condition:

$$e^{-2d\sqrt{E^2 - \tilde{k}^2 - m_{\text{II}}^2}} \left(\frac{ih_{\text{III}}\gamma^* - g_{\text{III}}}{g_{\text{III}} + ih_{\text{III}}\gamma} \right) = \frac{ig_I\gamma^* - h_I}{h_I + ig_I\gamma} \quad (\text{C3})$$

with $h_\alpha = \frac{\sqrt{E^2 - m_\alpha^2}}{E + m_\alpha} J_{\tilde{k} + \frac{1}{2}}(\sqrt{E^2 - m_\alpha^2}R)$, $g_\alpha = J_{\tilde{k} - \frac{1}{2}}(\sqrt{E^2 - m_\alpha^2}R)$ and $\gamma = \frac{\sqrt{E^2 - \tilde{k}^2 - m_{\text{II}}^2 + i\tilde{k}}}{E + m_{\text{II}}}$. When a localized flux is inserted through the origin, then away from origin, the solutions are still of the form given by (C1) with the replacement $\tilde{k} \rightarrow \tilde{k} + \Phi$ for Φ flux quanta. In this case, square integrability at the origin no longer constrains the coefficients in (C1), instead a matching to the solutions in the B-field region must be done. As discussed in the text, the simplest flux profile

allowing for analytical solution is to take a delta-function ring:²⁷ $B(r) = \Phi\delta(r - \epsilon)/(2\pi\epsilon)$. Then inside the ring, normalizability again constraints one coefficient to zero. Matching this at $r = \epsilon$ gives a required relation between the coefficients in the interior of the flux and the rest of the cap. Then the quantization condition is approximately as in (C3) with $\tilde{k} \rightarrow \tilde{k} + \Phi$ for $|\tilde{k} + \Phi| > 1/2$. For $|\tilde{k} + \Phi| \leq 1/2$ the explicit form of the B-field must be used to match wavefunctions at ϵ . The result can be summarized by making redefinitions in equation C3 (assuming $\Phi \geq 0$): $h_\alpha = \frac{\sqrt{E^2 - m_\alpha^2}}{E + m_\alpha} (d_1 J_{\tilde{k} + \frac{1}{2} + \Phi}(\sqrt{E^2 - m_\alpha^2}R) - d_2 J_{-\tilde{k} - \frac{1}{2} - \Phi}(\sqrt{E^2 - m_\alpha^2}R))$, $g_\alpha = d_1 J_{\tilde{k} - \frac{1}{2} + \Phi}(\sqrt{E^2 - m_\alpha^2}R) + d_2 J_{-\tilde{k} + \frac{1}{2} - \Phi}(\sqrt{E^2 - m_\alpha^2}R)$ where $d_1 = \frac{J_{\tilde{k} - 1/2} - d_2 J_{-\tilde{k} + 1/2 - \Phi}}{J_{\tilde{k} - 1/2 + \Phi}}$ $d_2 = \frac{J_{\tilde{k} - 1/2 + \Phi} J_{\tilde{k} + 1/2} - J_{\tilde{k} + 1/2 + \Phi} J_{\tilde{k} - 1/2}}{J_{-\tilde{k} - 1/2 - \Phi} J_{\tilde{k} - 1/2 + \Phi} - J_{-\tilde{k} + 1/2 - \Phi} J_{\tilde{k} + 1/2 + \Phi}}$ with all unspecified J s evaluated at $\sqrt{E^2 - M_\alpha^2}\epsilon$ so long as Φ is not an integer. For Φ integer, one further must replace $J_{-\tilde{k} \dots}$ to Y (the second Bessel function) and $-d_2$ to $+d_2$ in h_α .

* aselem@berkeley.edu

- ¹ L. Fu, C. L. Kane, and E. J. Mele, Phys. Rev. Lett. **98**, 106803 (2007).
- ² L. Fu and C. L. Kane, Phys. Rev. B **76**, 045302 (2007).
- ³ B. A. Bernevig, T. L. Hughes, and S.-C. Zhang, Science **314**, 1757 (2006).
- ⁴ B. A. Bernevig and S.-C. Zhang, Phys. Rev. Lett. **96**, 106802 (2006).
- ⁵ M. Knig, S. Wiedmann, C. Brne, A. Roth, H. Buhmann, L. W. Molenkamp, X.-L. Qi, and S.-C. Zhang, Science **318**, 766 (2007).
- ⁶ D. Hsieh, D. Qian, L. Wray, Y. Xia, Y. S. Hor, R. J. Cava, and M. Z. Hasan, NATURE **452**, 970 (2008).
- ⁷ Y. Xia, D. Qian, D. Hsieh, L. Wray, A. Pal, H. Lin, A. Bansil, D. Grauer, Y. S. Hor, R. J. Cava, and M. Z. Hasan, NATURE PHYSICS **5**, 398 (2009).
- ⁸ H. Zhang, C.-X. Liu, X.-L. Qi, X. Dai, Z. Fang, and S.-C. Zhang, Nature Physics **5**, 438 (2009).
- ⁹ R. Jackiw, Phys. Rev. **D29**, 2375 (1984).

- ¹⁰ A. J. Niemi and G. W. Semenoff, Phys. Rev. Lett. **51**, 2077 (1983).
- ¹¹ R. B. Laughlin, Phys. Rev. B **23**, 5632 (1981).
- ¹² B. I. Halperin, Phys. Rev. B **25**, 2185 (1982).
- ¹³ H. Nielsen and M. Ninomiya, Physics Letters B **130**, 389 (1983).
- ¹⁴ N. M. R. Peres, F. Guinea, and A. H. Castro Neto, Phys. Rev. B **73**, 125411 (2006).
- ¹⁵ V. P. Gusynin and S. G. Sharapov, Phys. Rev. Lett. **95**, 146801 (2005).
- ¹⁶ Y. L. Chen, J.-H. Chu, J. G. Analytis, Z. K. Liu, K. Igarashi, H.-H. Kuo, X. L. Qi, S. K. Mo, R. G. Moore, D. H. Lu, M. Hashimoto, T. Sasagawa, S. C. Zhang, I. R. Fisher, Z. Hussain, and Z. X. Shen, Science **329**, 659 (2010).
- ¹⁷ G. Rosenberg, H. M. Guo, and M. Franz, Phys. Rev. **B82**, 041104 (2010).
- ¹⁸ A. Selem, "The dirac equation and vielbein choice in polar decompositions," Preprint.

- ¹⁹ L. Fu and C. L. Kane, Phys. Rev. Lett. **100**, 096407 (2008).
- ²⁰ M. E. Peskin and D. V. Schroeder, *An Introduction To Quantum Field Theory (Frontiers in Physics)* (Westview Press, 1995).
- ²¹ R. Penrose and W. Rindler, *Spinors and Space-Time*, by Roger Penrose and Wolfgang Rindler, pp. 512. ISBN 0521347866. Cambridge, UK: Cambridge University Press, April 1988., edited by Penrose, R. & Rindler, W. (Cambridge University Press, 1988).
- ²² R. Jackiw and C. Rebbi, Phys. Rev. D **13**, 3398 (1976).
- ²³ T. Jaroszewicz, Phys. Rev. D **34**, 3128 (1986).
- ²⁴ J. Kiskis, Phys. Rev. D **15**, 2329 (1977).
- ²⁵ Y. Zhang, Y. Ran, and A. Vishwanath, Phys. Rev. B **79**, 245331 (2009).
- ²⁶ Y. Zhang and A. Vishwanath, Phys. Rev. Lett. **105**, 206601 (2010).
- ²⁷ M. G. Alford, J. March-Russell, and F. Wilczek, Nuclear Physics B **328**, 140 (1989).
- ²⁸ R. Jackiw and C. Rebbi, Phys. Rev. D **16**, 1052 (1977).
- ²⁹ M. Nakahara, *Geometry, Topology and Physics*, 2nd ed. (CRC Press, 2003).
- ³⁰ T. Eguchi, P. B. Gilkey, and A. J. Hanson, Phys. Rept. **66**, 213 (1980).